J Solid State Electrochem (2007) 11: 244–252
DOI 10.1007/s10008-006-0099-x

ORIGINAL PAPER

M. M. Abou-Krisha · F. H. Assaf · A. A. Toghan

Electrodeposition of Zn–Ni alloys from sulfate bath

Received: 12 October 2005 / Revised: 21 November 2005 / Accepted: 9 January 2006 / Published online: 18 February 2006

Abstract The electrodeposition of zinc–nickel (Zn–Ni) alloys from sulfate baths has been studied at different deposition times and H_2SO_4 and $NiSO_4$ concentrations; various characteristics have been observed during alloy deposition and dissolution. The deposit has been investigated by using scanning electron microscopy (SEM) and X-ray diffractometry. Cyclic voltammetry and galvanostatic measurements during electrodeposition have been conducted. Electrochemical and surface analysis indicate that deposition takes place with the formation of two different structures corresponding to γ-phase and δ-phase zinc–nickel alloys. During anodic part of the cyclic voltammetry of the alloys, a reduction process has been observed, which may be due to hydrogen evolution. With the increase of nickel concentration in the bath, the amount of γ-phase increases, as indicated by the relative increase in the height of the peaks in the X-ray patterns and anodic peaks in the cyclic voltammograms. Also, the corrosion resistance of the zinc–nickel alloy has been improved with an increased concentration of nickel. Under these experimental conditions the electrodeposition of the alloys is of anomalous type.

Keywords Anomalous codeposition · Zn–Ni alloy · Electrochemical studies · Electrodeposition

Introduction

The electrodeposition of zinc–nickel (Zn–Ni) coatings has attracted interest [1–4] on the account that these alloys are more corrosion resistant than pure zinc [5, 6]. Many studies have been attempted to understand the characteristics of this deposition process [7–14]. The electrodeposition of Zn–Ni is classified as a codeposition of anomalous type [15], where the less noble metal, zinc, deposits preferentially, and its percentage in the deposit is higher than that in the bath. There are some propositions which may explain the anomalous codeposition of the Zn–Ni alloys. Some of the scholars [15, 16] attribute the anomalous codeposition to a local pH increase near the cathode surface. This process is followed by the formation of zinc hydroxide precipitate and the inhibition of Ni^{2+} discharge. The proposition of another group is based on the under potential deposition (UPD) of zinc on nickel-rich zinc alloys or on nickel nuclei [17]. For corrosion protection, the alloy needs a low surface area with either a high content of Zn, which is less noble than steel (sacrificial film) or a high content of Ni, which is more noble than steel (barrier film).

Two other papers [18, 19] on NiFe electrodeposition propose different mechanisms. The mechanism of Lieder and Biallozor [18] assumes that Ni^{2+} discharges first to form a thin layer which chemisorbs water to form adsorbed Ni $(OH)^+$. Competition between the Ni^{2+} and Fe^{2+} to occupy active sites leads to the preferential deposition of Fe. Matlosz [19] uses a two-step reaction mechanism involving adsorbed monovalent intermediate ions for both electrodeposition of iron and nickel, as single metals, and combines the two to develop a model for codeposition. Anomalous effects have been assumed to be caused by preferential surface coverage due to differences in Tafel rate constants for electrodeposition.

Sasaki and Talbot [20] have proposed a model which extends the one-dimensional diffusion modeling of Grande and Talbot [21], a supportive or interpretive, rather than a predictive, model of electrodeposition. A main contribution of this model is the inclusion of hydrogen adsorption and its effects on electrodeposition. Zech et al. [22] have concluded that codeposition of iron group metals leads to a reduction of the reaction rate of the more noble component and an increase of the reaction rate of the less noble component compared to single metal deposition.

The aim of this work is to investigate the effect of $NiSO_4$ and H_2SO_4 concentrations in the plating bath and the deposition time on the alloy composition and its dissolution

M. M. Abou-Krisha (✉) · F. H. Assaf · A. A. Toghan
Faculty of Science, Chemistry Department,
South Valley University,
Qena, 83523, Egypt
e-mail: mortaga_aboukrisha@yahoo.com
Tel.: +20-105357605
Fax: +20-96-5211279

resistance. Selection of appropriate operating conditions, to obtain an optimum nickel amount that provides the best corrosion resistance of these types of alloy on steel substrate, have also been studied. The results of the experimental approach are essentially based on the analysis of the cathodic part of the cyclic voltammograms and galvanostatic measurements during electrodeposition. The linear polarization resistance technique and the anodic part of the cyclic voltammograms are used to elucidate the dissolution behavior of the given alloy. Scanning electron microscopy (SEM) and X-ray diffractometry are employed to examine the morphology of the deposited film, while atomic absorption is used to examine the deposit content.

Experimental

Experiments have been carried out by a three-electrode cell with a capacity of 100 cm^3. The electrolytes employed for electrodeposition of Zn–Ni alloys have been freshly prepared from Analar grade chemicals (used without further purification) dissolved in an appropriate volume of doubly distilled water. The standard chemical composition of electrolyte is 0.20 M $ZnSO_4$, 0.20 M $NiSO_4$, 0.01 M H_2SO_4, 0.40 M Na_2SO_4 and 0.16 M H_3BO_3 at 30.0°C and pH=2.5. The effects of variation of H_2SO_4 (0.005 to 0.05 M) and $NiSO_4$ concentrations (0.10 to 0.50 M) and the deposition time (1 to 20 min) have been investigated (Tables 1, 2 and 3). All experiments have been carried out in duplicate; the measurements have shown good reproducibility. For a standard bath deposition, series of experiments at different times were carried out and the relative standard deviation (RSD%) were found to be 4.8 and 6.4% for the Zn and Ni contents in the deposit, respectively.

Table 1 Values of Ni and Zn amount in the deposit, percentage of Ni and Zn content, current efficiencies percentage of the deposit, thickness, and electrochemical corrosion measurements of the deposit on steel (0.196 cm^2) from a bath containing 0.20 M $ZnSO_4$, different concentrations of $NiSO_4$, 0.01 M H_2SO_4, 0.40 M Na_2SO_4, and 0.16 M H_3BO_3 at 10 mA cm^{-2} for 10 min at 30.0°C

Ni^{2+} concentration in the bath/M	0.10	0.20	0.30	0.40	0.50
Ni amount in the deposit/10^{-6} g	14	36	41	47	55
Zn amount in the deposit/10^{-6} g	280	253	206	176	147
Ni content/%	4.8	12.5	16.6	21.1	27.2
Zn content/%	95.2	87.5	83.4	78.9	72.8
Zn–Ni deposit current efficiency (e_{total})/%	74.2	73.6	63.2	57.3	52.3
Thickness of the deposit/μm	2.08	2.01	1.69	1.52	1.35
I_{corr}/A $cm^{-2}\times10^{-3}$	4.44	4.28	4.21	4.13	4.05
R_p/kΩ	0.103	0.110	0.114	0.117	0.121
Corr. rate/ milli-inches $year^{-1}$	2.418	2.345	2.259	2.189	2.017
Corrosion potential (E_{corr})/V	−1.007	−0.997	−0.985	−0.974	−0.911

Cyclic voltammetric, galvanostatic, and anodic linear polarization resistance measurements have been done with an EG&G potentiostat\galvanostat Model 237A, which is controlled by a PC using 352 corrosion software. The zinc–nickel alloys produced during cathodic potentiodynamic technique (cathodic part of the cyclic voltammetry) onto a steel rod (working electrode) have been stripped under anodic potentiodynamic (anodic part of the cyclic voltammetry) conditions in the same plating bath.

The working electrode has mounted in a Teflon holder and has had a cross-sectional area of 0.196 cm^2. The reference electrode (a saturated Ag/AgCl/KCl) has mounted in a Luggin capillary, and a Pt sheet (6.0 cm^2) has been used as a counter electrode. The working electrode has been polished before each run by using successive grades of emery paper and degreased with ethyl alcohol before rinsing and drying. Before each run, the cell is cleaned with a chromic/sulfuric acid mixture followed by rinsing in distilled water. The cell is filled with 100 cm^3 of the electrolyte and is placed in a thermostatically controlled vessel maintained at 30.0°C.

The alloys obtained by depositing the metals galvanostatically at 10 mA cm^{-2} onto a steel rod have been used to measure the corrosion resistance and the composition of the deposit.

To measure the corrosion resistance of the deposit, the linear polarization technique is followed. The steel coated galvanostatically by Zn–Ni alloy has been washed and transferred into the electrolytic cell containing 100 cm^3 of 0.025 M HCl so as to dissolve the coating anodically. The sample is washed with doubly distilled water, and it is immediately put into the cell. Thus, after a few seconds (30 s), a steady corrosion potential has been reached. The anodic dissolution of deposits in a voltammetric mode is conducted at a potential scan rate of 2 mV s^{-1}. The values of electrochemical corrosion measurements of the coatings, E_{corr}—corrosion potential, I_{corr}—corrosion current, R_p—polarization resistance and corrosion rate, have been obtained and represented in Tables 1, 2 and 3. The corrosion potential (E_{corr}) is determined from the E vs log i plots. A shift in the corrosion potential towards more positive values emphasizes the increase of corrosion resistance.

The surface morphology of the deposit is evaluated by using a scanning electron microscope, (JSM-5500 LV, SEM, JEOL, Japan). Also, SEM has been used to measure the thickness of the deposits (cross-section). An X-ray diffractometer [(XRD) model D5000 Siemens diffractometer] is used to identify the phases of the Zn–Ni alloys deposited. The instrument is equipped with a copper anode generating Ni-filtered CuK_α radiation (λ=1.5418 Å, 40 kV, 30 mA). An on-line data acquisition and handling system have surely facilitated an automatic JCPDS library search and match (Diffrac software, Siemens) for phase identification purposes.

To determine the percentage of the electrodeposited composition, the deposit has been dissolved in 20 cm^3 of 3.0 M HNO_3 and then, diluted to 100 cm^3 with doubly

Table 2 Values of Ni and Zn amount in the deposit, percent Ni and Zn content, current efficiencies percentage of the deposit, thickness, and electrochemical corrosion measurements of the deposit on steel (0.196 cm^2) from a bath containing 0.20 M $ZnSO_4$, 0.20 M $NiSO_4$, different concentration of H_2SO_4, 0.40 M Na_2SO_4, and 0.16 M H_3BO_3 at 10 mA cm^{-2} for 10 min at 30.0°C

H_2SO_4 concentration in the bath/M	0.000	0.005	0.010	0.020	0.030	0.040	0.050
Ni amount in the deposit/10^{-6} g	46	47	50	43	30	25	19
Zn amount in the deposit/10^{-6} g	353	343	323	281	177	120	80
Ni content/%	11.5	12.1	13.4	13.3	14.5	17.2	19.1
Zn content/%	88.5	87.9	86.6	86.7	85.5	82.8	80.9
Zn–Ni deposit current efficiency (e_{total})/%	101.5	99.3	95.1	82.5	52.8	37.1	25.5
Thickness of the deposit/μm	2.77	2.71	2.58	2.24	1.43	0.99	0.68
I_{corr}/A $cm^{-2}\times10^{-3}$	4.18	4.15	4.12	4.22	4.27	4.34	4.41
R_p/kΩ	0.112	0.117	0.121	0.110	0.107	0.104	0.101
Corr. rate / milli-inches $year^{-1}$	2.241	2.213	2.187	2.255	2.301	2.367	2.398
Corrosion potential (E_{corr})/V	−1.006	−1.000	−0.983	−1.014	−1.017	−1.038	−1.044

distilled water. Then, a suitably diluted solution is analyzed to calculate the Zn and Ni contents in the deposited alloy by using Atomic Absorption Spectrometer (Varian SpectrAA 55). The Zn and Ni content in the deposit have been confirmed by EDS (Energy Dispersive X-ray Spectrometer) system with link Isis software and model 6587 An X-ray detector (OXFORD, UK). Using the resultant analysis, the film thickness and the cathode current efficiency of the deposit have been calculated.

The thickness of the deposited alloy layer has been approximately estimated from the amount of deposit and the densities of Zn (d_{Zn}=7.14 g cm^{-3}) and Ni (d_{Ni}=8.90 g cm^{-3}) of the same surface area (0.196 cm^2) [14, 17] and confirmed by SEM (cross-section). The experiments have been done without cathode movement or solution agitation.

Table 3 Values of Ni and Zn amount in the deposit, percent Ni and Zn content, current efficiencies percentage of the deposit, thickness, and electrochemical corrosion measurements of the deposit on steel (0.196 cm^2) from a bath containing 0.20 M $ZnSO_4$, 0.20 M $NiSO_4$, 0.01 M H_2SO_4, 0.40 M Na_2SO_4, and 0.16 M H_3BO_3 at 10 mA cm^{-2} for different deposition time at 30.0°C

Deposition time/min	1	5	10	15	20
Ni amount in the deposit/10^{-6} g	0	22	41	53	67
Zn amount in the deposit/10^{-6} g	17	134	266	386	500
Ni content/%	0	14.1	13.4	12.1	11.8
Zn content/%	100	85.9	86.6	87.9	88.2
Zn–Ni deposit current efficiency (e_{total})/%	43.4	79.6	78.3	74.5	72.1
Thickness of the deposit/μm	0.12	1.08	2.12	3.05	3.94
I_{corr}/A $cm^{-2}\times10^{-3}$	4.96	4.45	4.23	4.11	4.03
R_p/kΩ	0.87	0.102	0.111	0.114	0.120
Corr. rate/milli-inches $year^{-1}$	3.132	2.534	2.255	2.178	2.023
Corrosion potential (E_{corr})/V	−1.015	−1.006	−0.996	−0.990	−0.974

Results and discussion

Effect of nickel concentration

The influence of Ni^{2+} concentration in the electrolyte on the cathodic polarization part of the cyclic voltammograms is studied (Fig. 1). The deposition potentials are shifted positively with increasing Ni^{2+} concentration. Also, the cathodic peak current which starts at −0.5 V, probably attributable to hydrogen evolution [14], decreases with increasing Ni^{2+}concentration. This is due to the competitive adsorption between Ni^{2+} and H^+ to occupy active sites leading to the preferential adsorption of nickel intermediate with Ni^{2+} concentration increases [18–22].

The phases in the Zn–Ni alloys have varied with nickel concentration and identified by X-ray diffraction (Fig. 2). Figure 2a (at 0.10 M Ni^{2+}) and 2b (at 0.50 M) indicate that the increase in Ni^{2+} concentration leads to an increase in the γ-phase and a decrease in δ-phase. This means that the relative amount of γ- and δ-phases in the deposits (indicated from the peak heights) depend on the nickel content in the electrodeposited alloy.

The cyclic voltammograms are a convenient spectrum-like diagram depicting the various phases that are exposed during corrosion of the deposit [23]. The voltammograms in Fig. 1 consist of two anodic peaks. The first dissolution anodic peak (at −0.97 V) corresponds to the dissolution of Zn from δ-(Ni_3Zn_{22}) phase, which shifts positively; the peak height decreases with increasing Ni^{2+} concentration. The second peak has appeared at about −0.64 V and is attributable to the dissolution of Zn from γ-(Ni_5Zn_{21}) phase; its height increases with Ni^{2+} concentration [23, 24]. This means that the increase of nickel concentration in the bath causes an increase in γ-phase and a decrease in δ-phase.

The results of galvanostatic measurements (Fig. 3) show that there is some potential trembling at low Ni^{2+} concentration. This is probably due to the bubbles of hydrogen, which increases at low Ni^{2+} concentration, blocking part of the electrode surface [25]. The potential trembling decreases when Ni^{2+} concentration increases. Inspection of Fig. 3 reveals an appreciable decrease in cathodic deposition potential of the alloy as the Ni^{2+} concentration increases in

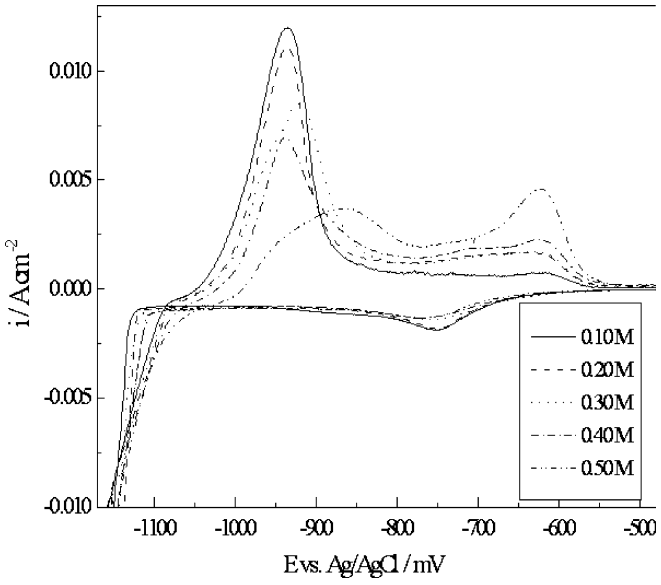

Fig. 1 *i–E* curves (cyclic voltammograms) for steel in 0.20 M $ZnSO_4$, different concentrations of $NiSO_4$, 0.01 M H_2SO_4, 0.40 M Na_2SO_4, 0.16 M H_3BO_3, and scan rate of 5 mV s^{-1} at 30.0°C

the plating bath. Obviously, during the deposition of Ni, low overpotential is needed to create the initial nucleus [7] with the increase of Ni^{2+} concentration.

Figure 4 shows the SEM micrographs obtained under similar conditions. It is quite clear that a non-uniform deposit is obtained in the bath at the concentration of 0.10 M Ni^{2+} (Fig. 4a). This is probably due to the higher Zn content in the deposited film. Kalantary et al. [26] have reached similar micrographs for pure Zn electrodeposition. The most uniform deposit with a small grain size is observed as the Ni^{2+} concentration is raised to 0.50 M (Fig. 4b).

Table 1 shows that high concentration of Ni^{2+} in the bath has increased nickel content in the deposit, while Zn content, total mass and current efficiency and thickness of the deposited layer are decreased. Decrease of the deposited thickness is perhaps related to the decrease of Zn content in the alloy, which represents the main alloy component of low density.

Linear polarization tests have been made employing a steel coated galvanostatically by Zn–Ni alloy (Fig. 5). From this figure the corrosion potential (E_{corr}) is determined (Table 1). The corrosion potential is, however, an indication of the activity of the deposit in a corrosive environment. E_{corr} is shifted positively (i.e., the corrosion resistance increase)

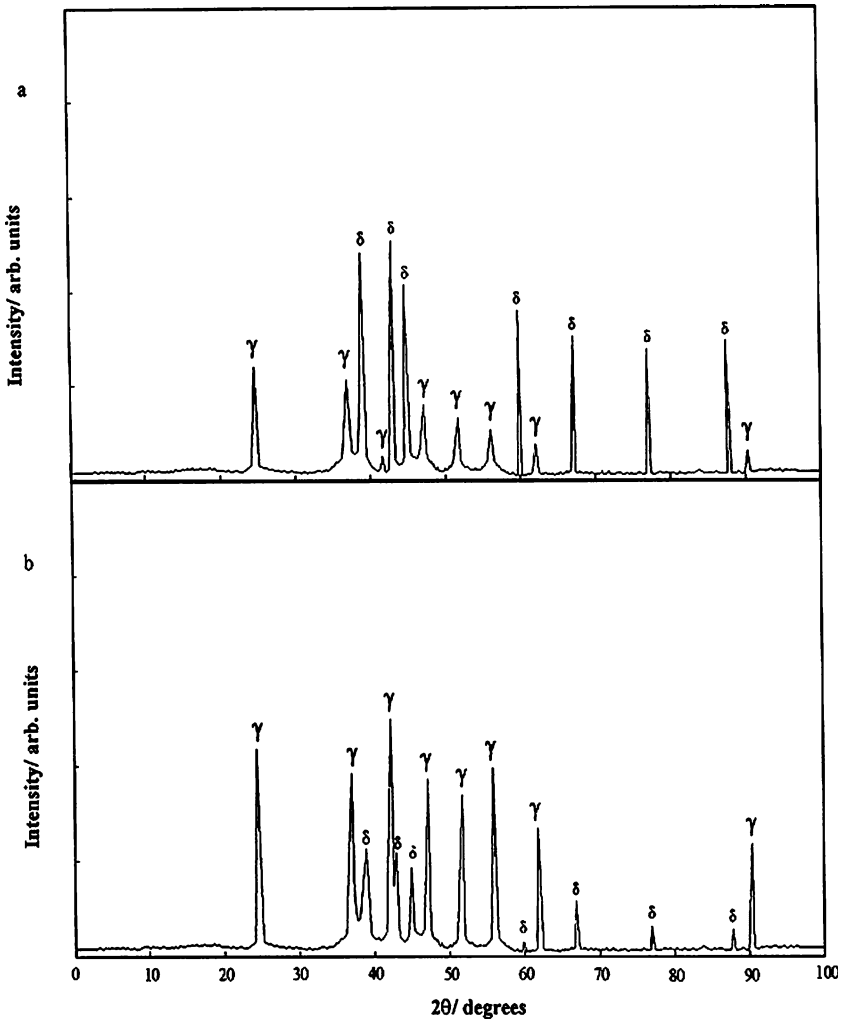

Fig. 2 XRD patterns of electrodeposited Zn–Ni on steel, obtained at a potential of −1.13 V holds for 15 min, from a bath containing 0.20 M $ZnSO_4$, different concentrations of $NiSO_4$, 0.01 M H_2SO_4, 0.40 M Na_2SO_4, and 0.16 M H_3BO_3 at 30.0°C. **a** at 0.10 M Ni^{2+}; **b** at 0.50 M Ni^{2+}

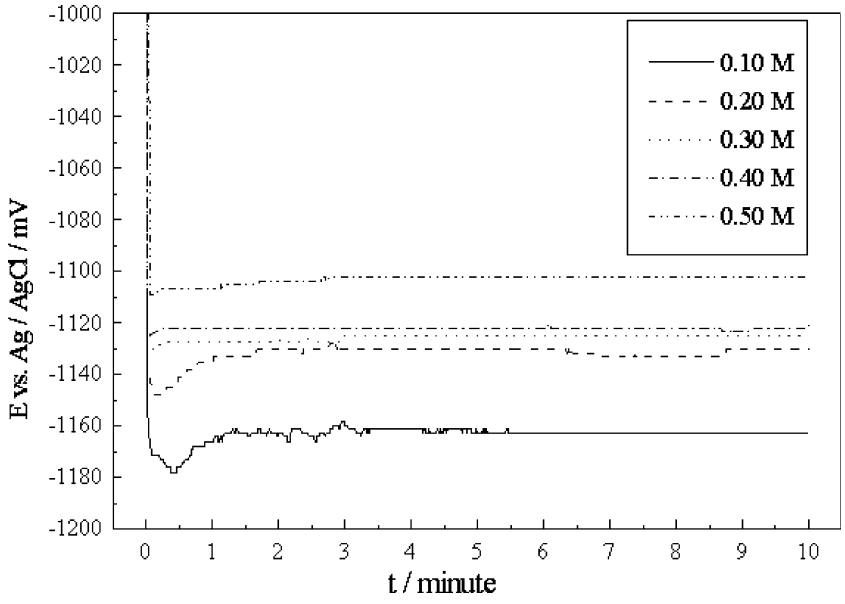

Fig. 3 *E–t* curves for steel in 0.20 M $ZnSO_4$, different concentrations of $NiSO_4$, 0.01 M H_2SO_4, 0.40 M Na_2SO_4, and 0.16 M H_3BO_3 at 10 mA cm^{-2} for 10 min at 30.0°C

with increasing Ni^{2+} concentration, compared with the higher negative values (E_{corr}=−1.062 V) for electrodeposited pure Zn on steel [26]. It seems that when increasing Ni_2SO_4 concentration, the corrosion rate and current have decreased and polarization resistance has increased. This indicates that corrosion resistance has increased by increasing the Ni_2SO_4 concentration. Depending on the above results, one may select an appropriate operating conditions to obtain an optimum nickel amount in the range of 11–13% that provides acceptable corrosion resistance for these types of alloy on steel substrate [27–29].

Effect of sulfuric acid concentration

Figure 6 shows the influence of H_2SO_4 concentration (0.0–0.05 M) in the plating bath on the potentiodynamic cathodic polarization curves. These curves have displayed that the deposition potentials are shifted positively with increasing H_2SO_4 concentration. It appears from Table 2 that the amount of deposited Zn and Ni decreases with increasing H_2SO_4, while the Ni content in the deposit increases, but Zn content decreases under similar conditions. Also, the thickness of the deposit decreases with the increase in H_2SO_4concentration. The positive shifting of the deposition potential, at high H_2SO_4concentration, may be the reason for the increase of Ni content. Figure 6 also shows that there is a trembling in the potential–current curves at mostly high H_2SO_4concentration, which increases with the increase of H_2SO_4concentration in the bath. On the other hand, the cathodic peak that approximately started at −0.5 V is shown only in the presence of H_2SO_4, and it increases with increasing concentration of H_2SO_4 as a result of high hydrogen evolution.

Anodic sweep in cyclic voltammetric studies for Zn–Ni alloys is represented graphically in Fig. 7. From the bath, in the absence of H_2SO_4, a single anodic peak, which is attributable to the Zn dissolved from δ-phase of low maximum, is observed at about −0.92 V, although there is a higher content of Zn in the deposit. This has to do with the absence of H_2SO_4, which acts as a corrosive medium and aids to increase the dissolution process. Furthermore, there is no reduction peak during the anodic polarization process. Moreover, reduction peaks have been observed in the

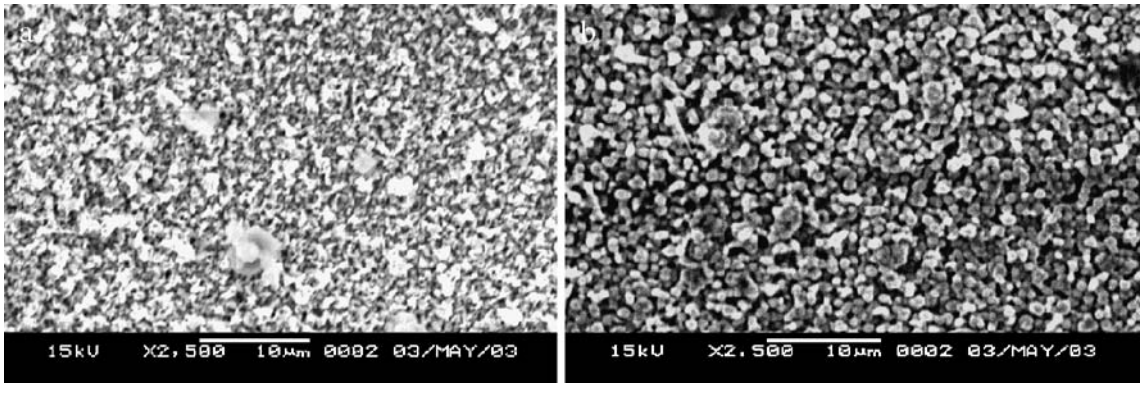

Fig. 4 SEM photographs of electrodeposited Zn–Ni on steel from a bath containing 0.20 M $ZnSO_4$, different concentrations of $NiSO_4$, 0.01 M H_2SO_4, 0.40 M Na_2SO_4, and 0.16 M H_3BO_3 at 10 mA $cm^{-2}$for 10 min at 30.0°C. **a** at 0.10 M Ni^{2+}; **b** at 0.50 M Ni^{2+}

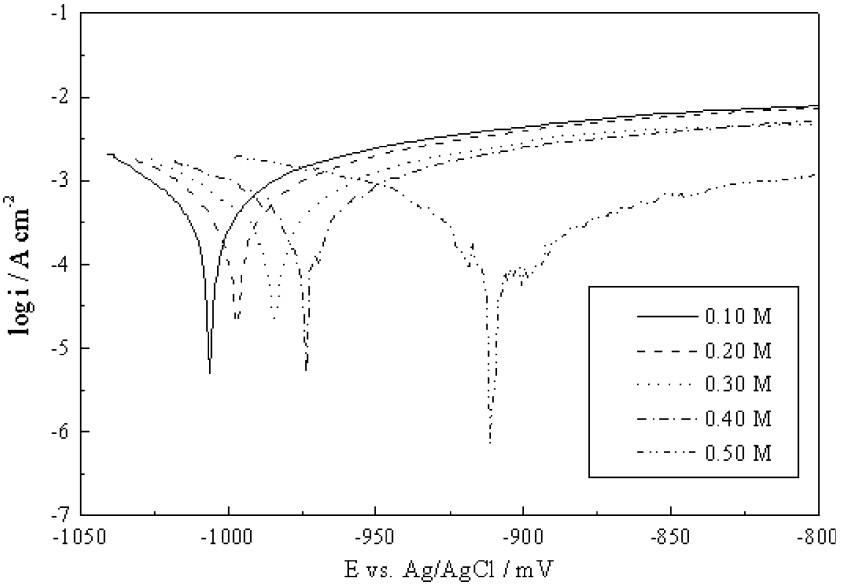

Fig. 5 log *i*–*E* curves for steel, plated from a bath containing 0.20 M $ZnSO_4$, different concentrations of $NiSO_4$, 0.01 M H_2SO_4, 0.40 M Na_2SO_4, and 0.16 M H_3BO_3 at 10 mA $cm^{-2}$for 10 min at 30.0°C, in 0.025 M HCl at 30.0°C

presence of H_2SO_4, and their height has increased by raising the concentration of H_2SO_4 in the bath. A reduction peak during the oxidation of zinc–nickel alloys was observed in other cases [30], and this was attributed to hydrogen evolution due to the low pH values used in that cases and in this study, too. However, in another study which uses weakly acidic medium [7], the results indicated that the observed reduction process during the oxidation of zinc–nickel alloys corresponds to the deposition of nickel, together with some hydrogen evolution.

At a concentration of 0.01 M H_2SO_4, two anodic peaks have appeared as a result of the dissolution of Zn from two different phases: δ (first anodic peak) and γ (second dissolution peak). The second peak disappeared in the presence of higher concentrations (>0.01 M) of H_2SO_4. This observation is corroborated by X-ray diffraction which manifested the formation of two phases when 0.01 M H_2SO_4 is added. The addition of 0.03 M H_2SO_4, however, has produced one phase (δ-phase). Moreover, the peak height of δ-phase has decreased when the acid concentration increased in the bath. These results may be ascribed to the decrease of Zn concentration in the deposited film; conversely, the δ-phase and corrosion resistance of the alloy have decreased. The reason of the reduction in the amount of Zn, with higher concentration of H_2SO_4, is due to the competing factor in anomalous codeposition enabling near normal deposition of nickel to occur.

Galvanostatic measurements (Fig. 8) reveal that the increase of H_2SO_4 concentration (0.005 to 0.05 M) in the plating bath generally decreases the cathodic deposition potential of the alloy, whereas, the lowering of the overpotential that is needed to create the initial nuclei makes the deposition process easier. This is due to the addition of H_2SO_4. But, in the absence of H_2SO_4, higher overpotential is needed to create the initial nuclei.

As a result, the morphology of the deposit has changed from small grain size in the absence of sulfuric acid (Fig. 9a)

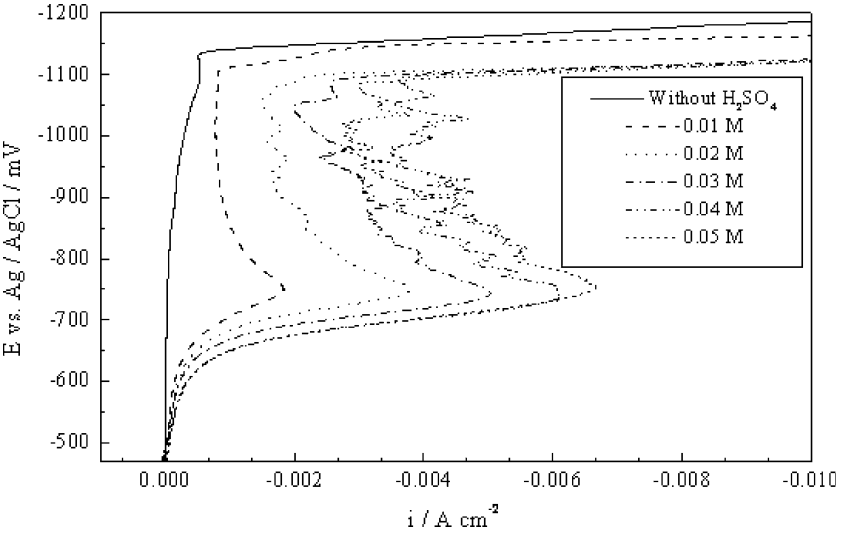

Fig. 6 *E*–*i* curves for steel in 0.20 M $ZnSO_4$, 0.20 M $NiSO_4$, different concentrations of H_2SO_4, 0.40 M Na_2SO_4, 0.16 M H_3BO_3, and scan rate of 5 mV s^{-1} at 30.0°C

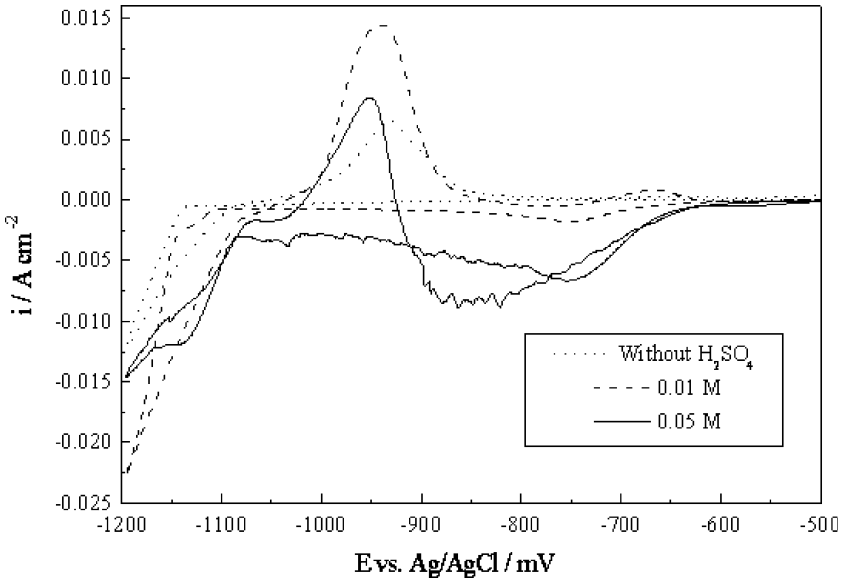

Fig. 7 *i–E* curves (cyclic voltammograms) for steel in 0.20 M $ZnSO_4$, 0.20 M $NiSO_4$, different concentrations of H_2SO_4, 0.40 M Na_2SO_4, 0.16 M H_3BO_3, and scan rate of 5 mV s^{-1} at 30.0°C

into a uniform fine grain size in its existence (Fig. 9b). It is also observed that the deposit suffers from holes and voids at concentrations of H_2SO_4 higher than 0.01 M in the plating bath (Fig. 9c). This may go back to the high hydrogen evolution.

From the fundamental theory of nucleation and growth process, it is realized that both the nucleation and the growth rates are potential dependent [31]. In the case of Zn–Ni alloys deposited at high overvoltage, the growth rate exceeds the nucleation rate, producing small grain size film, as observed in Fig. 9a. At a lower overvoltage, a transition occurs as the nucleation rate exceeds the growth rate of the alloy. This is due to the addition of H_2SO_4, which causes the formation of fine grain films (Fig. 9b). At a high concentration of H_2SO_4, a non-uniform deposit is observed (Fig. 9c). In conclusion, the suitable concentration of H_2SO_4 needed to achieve better surface coverage with fine grained structure is about 0.01 M. It is obvious that the formed fine grain films means that the nucleation density of the deposit increased, raised the Ni amount in the alloy, and the surface coverage is better, and in turn, the corrosion resistance increases.

Table 2 demonstrates the E_{corr} calculated from anodic polarization curves of the examined alloys (coated on steel in baths containing different H_2SO_4 concentrations) in 0.025 M HCl. These results reveal that E_{corr} has positively shifted at lower concentrations (or in the absence) of H_2SO_4. This may be attributed to the rise of the amount of Ni in the deposit at low sulfuric acid concentration. It is important to mention that in Table 1, E_{corr} is shifted positively with a higher amount and content of nickel. Similarly, in Table 2 E_{corr} has shifted positively with a higher amount of nickel, but shifted negatively with a higher nickel content because of a decrease of the amount of Zn and Ni. In addition, the data has indicated that the current efficiency of the alloy decreases with a higher H_2SO_4 concentration due to the increase of the hydrogen evolution. Also, it is obvious that the corrosion rate and current have decreased, and polarization resistance has increased with the amount of Ni increased.

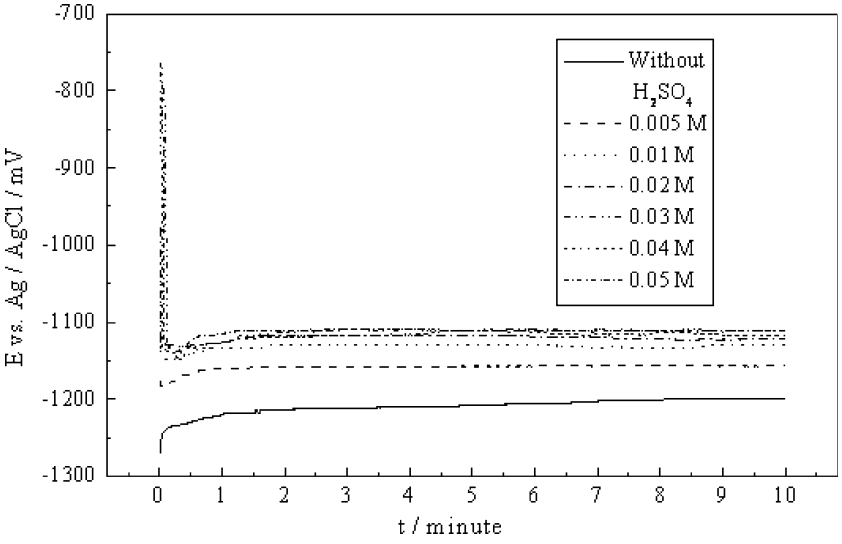

Fig. 8 *E–t* curves for steel in 0.20 M $ZnSO_4$, 0.20 M $NiSO_4$, different concentrations of H_2SO_4, 0.40 M Na_2SO_4, and 0.16 M H_3BO_3 at 10 mA cm^{-2} for 10 min at 30.0°C

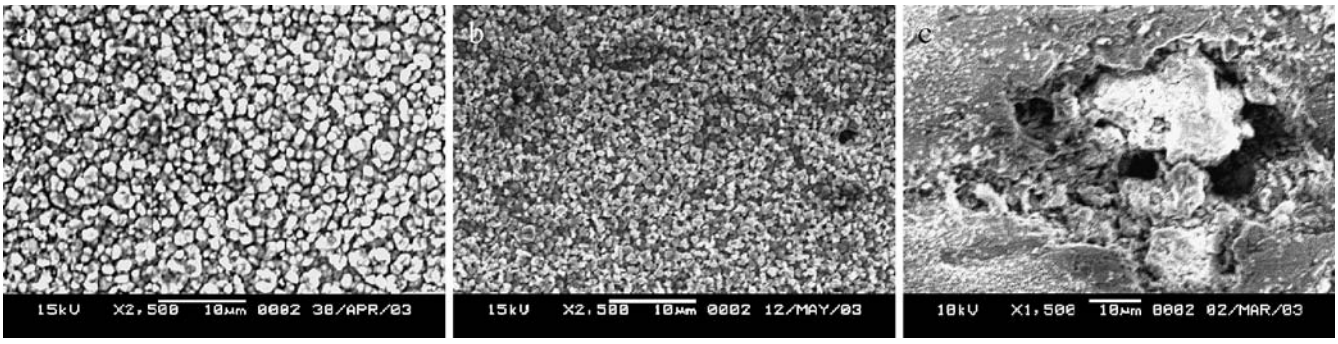

Fig. 9 SEM photographs of electrodeposited Zn–Ni on steel from a bath containing 0.20 M $ZnSO_4$, 0.20 M $NiSO_4$, different concentrations of H_2SO_4, 0.40 M Na_2SO_4, and 0.16 M H_3BO_3 at 10 mA $cm^{-2}$for 10 min at 30.0°C. **a** Bath without H_2SO_4; **b** at 0.01 M. **c** at 0.03 M

Effect of deposition time

Figure 10 shows the cyclic voltammetric behavior of the studied alloys by using different deposition time (by different sweeping rate). It is quite clear from the cathodic part of this figure that the cathodic peaks, starting approximately at −0.5 V, increase when the deposition time decreases; meanwhile, the sweeping rate increases. The decrease of deposition time has also shifted the deposition potential negatively. This is because the adsorbed Ni^{2+} and $Zn^{2+}$are less than the adsorbed H^+ at the beginning (lower deposition time), which leads to a decrease of Ni and Zn amount in the deposit. Figure 10 shows that two peaks are obtained for the Zn oxidation at about −0.9 and −0.7 V at high deposition time (1 and 5 mV s^{-1}) in the potentiodynamic anodic polarization. This means that at higher deposition time, the two phases are formed. At short deposition time, the second peak disappears, and only one oxidation peak is observed, which is mainly caused by the dissolution of Zn from δ-phase or Zn deposit alone. It appears that the height of the first peak has increased when the deposition time decreases, owing to the decrease of Ni concentration in the deposit, which aids to inhibit the dissolution of Zn deposit. Furthermore, the start of the first anodic peak has positively shifted with the increase of the deposition time, as a result of the increase of the corrosion resistance of the alloy. From X-ray diffraction analysis of the coatings, obtained at high deposition time, it is clear that the deposit consisted of two phases. On the other hand, δ-phase/enriched zinc alloy is deposited at low deposition time.

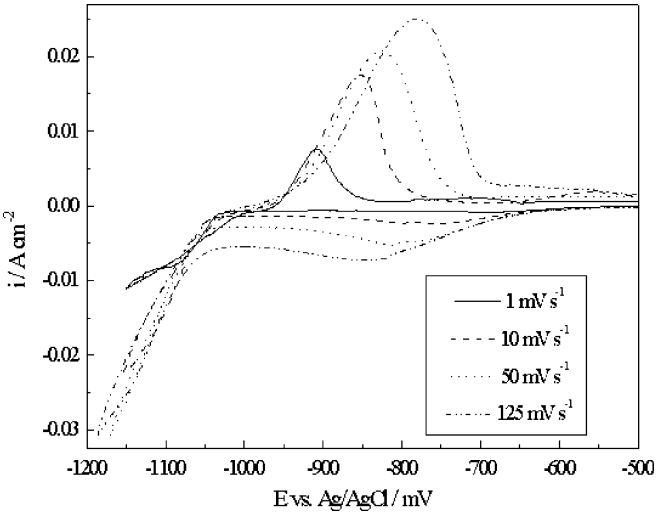

Fig. 10 *i–E* curves (cyclic voltammograms) for steel in 0.20 M $ZnSO_4$, 0.20 M $NiSO_4$, 0.01 M H_2SO_4, 0.40 M Na_2SO_4, 0.16 M H_3BO_3, and different scan rates at 30.0°C

After 1 min, the deposit is enriched with Zn (Table 3). This indicates that a high Zn amount is deposited, and the initial layer consisted mainly of Zn (anomalous codeposition). It is also obvious that at low deposition time there is more hydrogen evolution. The current efficiency has decreased due to the decrease of the concentration of both Ni^{2+} and Zn^{2+} with the passing time. This means that absolute amounts of deposits have increased while the relative ones are decreased. The obtained data show that the thickness of the deposited layer has increased (0.12→3.94 μm) when the deposition time increases (1–20 min). Table 3 also shows that the corrosion potential, rate, and current have decreased and polarization resistance has increased as the deposition time increases.

Conclusions

The electrodeposition of Zn–Ni alloys from sulfate bath, with different deposition times, and concentration of nickel and sulfuric acid have been studied. Under the examined conditions, the electrodeposition of the alloys belonged to the anomalous type. When the nickel concentration in the bath is maintained between 0.10 and 0.50 M, deposits with nickel content of 4.8–27.2% have been produced. X-ray diffraction studies have revealed that the alloys consist of the δ-phase or a mixture of the two phases, δ and γ, in relation to the different variables. From SEM, it may be concluded that fine grains can be obtained with a bath containing 0.50 M Ni^{2+} and 0.01 M H_2SO_4 concentrations at long deposition time. This contributes to the enhancement of corrosion resistance.

The amount of deposited Zn and Ni and the thickness of the deposit have decreased when H_2SO_4 increases, but at the same time, the relative amount of Ni in the deposit increases when Zn decreases under the same conditions. Furthermore,

by adding H_2SO_4, a reduction peak is observed during the potentiodynamic oxidation of these alloys.

At 1 min, the deposit is enriched with Zn, which indicates that a high amount of Zn is deposited, and the initial layer consists mainly of Zn (anomalous codeposition). Also, it appears that at short deposition time, more hydrogen evolution is observed.

References

1. Brooks I, Erb U (2001) Scr Mater 44:853
2. Bajat JB, Kacarevic-Popovic Z, Miskovic-Stankovic VB, Maksimovic MD (2000) Progr Org Coat 39:127
3. Muller C, Sarret M, Benballa M (2002) J Electroanal Chem 519:85
4. Beltowska-Lehman E, Ozga P, Swiatek Z, Lupi C (2002) Surf Coat Technol 151:444
5. Crotty D (1996) Met Finish 94:54
6. Roventi G, Fratesi R, della Guardia RA, Barucca G (2000) J Appl Electrochem 30:173
7. Muller C, Sarret M, Benballa M (2001) Electrochim Acta 46:2811
8. Barcelo G, Garcia J, Sarret M, Muller C, Pregonas J (1994) J Appl Electrochem 24:1249
9. Elkhatabi F, Sarret M, Muller C (1996) J Electroanal Chem 404:45
10. Elkhatabi F, Barcelo G, Sarret M, Muller C (1996) J Electroanal Chem 419:71
11. Fabri Miranda FJ, Barcia OE, Mattos OR, Wiart R (1997) J Electrochem Soc 144:3441
12. Elkhatabi F, Benballa M, Sarret M, Muller C (1999) Electrochim Acta 44:1645
13. Koura N, Suzuki Y, Idemoto Y, Kato T, Matsumoto F (2003) Surf Coat Technol 169:120
14. Abou-Krisha M (2005) J Appl Surf Sci 252:1035
15. Brenner A (1963) Electrodeposition of alloys, vols 1 and 2. New York, Academic p 194
16. Ashassi-Sorkhabi H, Hagrah A, Parvini-Ahmadi N, Manzoori (2001) Surf Coat Technol 140:278
17. Ohtsuka T, Kuwamura E, Komori A, Uchida T (1995) ISIJ Int 35:892
18. Lieder M, Biallozor S (1998) Surf Coat Technol 26:23
19. Matlosz M (1993) J Electrochem Soc 140:2272
20. Keith Sasaki Y, Talbot BJ (2000) J Electrochem Soc 147:189
21. Grande WC, Talbot JB (1993) J Electrochem Soc 140:675
22. Zech N, Poldlaha EJ, Landolt D (1999) J Electrochem Soc 146:2886
23. Wu Zhongda, Fedrizzi L, Bonora PL (1996) Surf Coat Technol 85:170
24. Ramacha TL r, Panikkar SK (1960) Electroplating Met Finish 13:405
25. Velichenko AB, Portillo J, Alcobe X, Sarret M, Muller C (2000) Electrochim Acta 46:407
26. Kalantary MR, Wilcox GD, Gabe DR (1998) Br Corros J 33:197
27. Waston SA (March 1988) Nickel development Institute Publications, Report No 13001, Watson SA (April 1991) Proceedings of IMF Conference, Torquay 61–78
28. Short N, Abibsi A, Dennis JK (1989) Trans IMF 67:73
29. Short N, Abibsi A, Dennis JK (1991) Trans IMF 69:145
30. Lin Y, Selman JR (1993) J Electrochem Soc 123:55
31. Karwas C, Hepel T (1989) J Electrochem Soc 136:1672